Available online at www.sciencedirect.com
SCIENCE DIRECT®
Journal of Colloid and Interface Science 274 (2004) 607–612
JOURNAL OF Colloid and Interface Science
www.elsevier.com/locate/jcis

Angstrom-to-millimeter characterization of sedimentary rock microstructure

A.P. Radlinski,[a,*] M.A. Ioannidis,[b] A.L. Hinde,[a] M. Hainbuchner,[c] M. Baron,[d] H. Rauch,[c] and S.R. Kline [e]

[a] *Geoscience Australia, GPO Box 378, Canberra City, Australian Capital Territory 2601, Australia*
[b] *Department of Chemical Engineering, University of Waterloo, Waterloo, ON, Canada*
[c] *Atominstitut der Österreichischen Universitäten, Vienna, Austria*
[d] *Institute Max von Laue–Paul Langevin, Grenoble Cedex, France*
[e] *NIST Center for Neutron Research, Gaithersburg, MD, USA*

Received 21 August 2003; accepted 6 February 2004

Available online 9 April 2004

Abstract

Backscatter SEM imaging and small-angle neutron scattering (SANS) data are combined within a statistical framework to quantify the microstructure of a porous solid in terms of a continuous pore-size distribution spanning over five orders of magnitude of length scale, from 10 Å to 500 μm. The method is demonstrated on a sample of natural sandstone and the results are tested against mercury porosimetry (MP) and nuclear magnetic resonance (NMR) relaxation data. The rock microstructure is fractal ($D = 2.47$) in the pore-size range 10 Å–50 μm and Euclidean for larger length scales. The pore-size distribution is consistent with that determined by MP. The NMR data show a bimodal distribution of proton T_2 relaxation times, which is interpreted quantitatively using a model of relaxation in fractal pores. Pore-length scales derived from the NMR data are consistent with the geometrical parameters derived from both the SEM/SANS and MP data. The combined SANS/BSEM method furnishes new microstructural information that should facilitate the study of capillary phenomena in hydrocarbon reservoir rocks and other porous solids exhibiting broad pore-size distributions.

Keywords: Porous materials; Pore size; Small-angle scattering; Fractals; Magnetic resonance; Mercury porosimetry

1. Introduction

To understand and model the behavior of fluids confined in porous solids, as required in a plethora of engineering applications [1,2], one would like to have a complete picture of pore geometry—a picture in which the smallest as well as the largest pore-length scales are quantitatively represented. This is particularly challenging for sedimentary rocks, which occupy an extremely broad distribution of length scales (from nanometers to hundreds of micrometers). The need to account quantitatively for pore-length scales on the order of grain size and for the finer structural features of the rock–pore interface is evident in efforts to predict the amount of capillary-bound fluids [3,4], the dependence of electrical resistivity and relative permeability on water saturation [5], and the rate of spontaneous imbibition [6].

The microstructure of sedimentary rocks was extensively studied in the 1980s, when the connection was made between fractal geometry [7] and the microstructure of heterogeneous surfaces [8]. Katz and Thompson [9] used SEM and optical microscopy to demonstrate the fractal character of pore space in sandstones over length scales ranging from 0.1 to 100 μm. This was followed by a series of papers on the microgeometry of shales, sandstones, and carbonates, which established that the upper size limit for fractal microstructures varies in the range from 5 to 100 μm, depending on rock lithology [10,11]. Other studies on fractal features of sandstone and limestone rocks include the works of Jacquin and Adler [12] and Hansen and Skjeltorp [13], who used optical microscopy to determine the fractal volume and surface dimensions. Bale and Schmidt

* Corresponding author.
E-mail address: andrzej.radlinski@ga.gov.au (A.P. Radlinski).

0021-9797/$ – see front matter
doi:10.1016/j.jcis.2004.02.035

[14] derived the analytical form of the correlation function for surface fractals and applied it to the analysis of small-angle X-ray scattering (SAXS) data on lignite coals. The expression for the correlation function was later modified by Mildner and Hall [15] to account for the limited size of real fractal objects and by Wong and Bray [16] to account for finite scattering as the fractal dimension approaches a value of 3. Wong et al. [17] used small-angle neutron scattering (SANS) to study the microstructure of sandstone, shale, limestone, and dolomite samples over length scales ranging from 5 to 500 Å. They found a nonuniversal fractal character in sandstones and shales, which they attributed to the varying clay content of the samples. Cohen [18] presented a theoretical model of various morphological regimes in sedimentary rocks and explained suppressed grain sintering and formation of rough grain–pore interfaces as the consequence of small pore–grain free energy by comparison to the grain-boundary free energy. There is an extensive body of work applying measurements of adsorption isotherms to determine the fractal dimensions of solid adsorbents. These methods have been reviewed by Avnir [19] and, more recently, by Terzyk et al. [20].

Although the rock–pore interface has extensive fractal properties, fractal scaling laws cannot describe the microstructure over all relevant length scales. In fact, porous sedimentary rocks have both Euclidean and fractal characteristics. Their internal architecture can be completely described neither as a collection of compacted grains [21] nor as a surface fractal. Quantifying the entire spectrum of pore length scales is very difficult. On one hand, direct imaging methods such as backscatter scanning electron microscopy (BSEM) [22,23], X-ray microtomography [24], or confocal laser microscopy [25] cannot provide statistically significant microstructure data at length scales much smaller than about 1 μm. On the other hand, indirect imaging methods such as small-angle and ultra-small-angle neutron scattering (SANS and USANS), yield the volume-averaged Fourier transform of the density correlation function on length scales ranging from 1 nm to about 10 μm [26]. Greater length scales, accounting for much of the pore volume in sedimentary rocks, cannot be probed by these techniques.

In this paper we combine SANS and USANS measurements with BSEM-derived correlation information to image, in Fourier reciprocal space, the entire void space within sedimentary rock. The experiments performed and the theory behind the fusion and subsequent analysis of combined SANS/USANS/BSEM data are described in Section 2. Application of these methods to a sample of reservoir sandstone is discussed in Section 3, where it is shown that the pore-size distribution derived using a polydisperse spherical pore (PDSP) model is quantitatively consistent with structural information obtained by mercury porosimetry (MP) and nuclear-magnetic-resonance (NMR) relaxometry. Key findings and implications for future work are summarized in Section 4.

2. Materials and methods

2.1. Statistical fusion and analysis of imaging and scattering data

A porous medium is quite generally described in terms of a binary phase function $Z(\mathbf{x})$, taking the value of unity if $\mathbf{x}$ points to void and zero otherwise [27]. Statistical properties of $Z(\mathbf{x})$, directly accessible from binary BSEM images, are the porosity $\phi = \langle Z(\mathbf{x})\rangle$ and the correlation function $R_z(\mathbf{r}) = \langle Z(\mathbf{x})Z(\mathbf{x}+\mathbf{r}) - \phi^2\rangle / I(\phi - \phi^2)$, where $\mathbf{r}$ is a lag vector and angular brackets denote averaging [22,23]. For isotropic media, the correlation function depends only on the modulus r of the lag vector $\mathbf{r}$; i.e., $R_z(\mathbf{r}) = R_z(r)$. In SANS/USANS of rocks, which scatter neutrons as a quasi-two-phase system [26], the measured scattering intensity $I(Q)$ is the Fourier transform of the correlation function,

$$I(Q) = 4\pi(\Delta\rho)^2(\phi - \phi^2)\int_0^\infty r^2 R_z(r)\frac{\sin(Qr)}{Qr}\,dr, \tag{1}$$

where $(\Delta\rho)^2$ is the scattering length density contrast and the magnitude of the scattering vector $Q = 4\pi\sin(\theta/2)/\lambda$, where θ and λ are the scattering angle and beam wavelength, respectively. For periodic structures the magnitude of the scattering vector is related to the characteristic size as $Q = 2\pi/r$. Statistical analysis of binary BSEM images provides $R_z(r)$ and, by virtue of Eq. (1), $I(Q)$ in the range $10^{-7} < Q < 10^{-4}$ Å^{-1}. This range overlaps with and extends the range accessible by the combined SANS/USANS data ($10^{-5} < Q < 10^{-1}$ Å^{-1}). In the extended range 10 Å $< r < 1$ mm, the correlation function is then recovered from the extended $I(Q)$ data by the equation

$$R_z(r) = \frac{1}{2\pi^2(\Delta\rho)^2(\phi - \phi^2)}\int_0^\infty Q^2 I(Q)\frac{\sin(Qr)}{Qr}\,dQ, \tag{2}$$

whereas the porosity ϕ is obtained from the invariant Y, defined as follows:

$$Y \equiv \int_0^\infty Q^2 I(Q)\,dQ = 2\pi^2(\Delta\rho)^2\phi(1-\phi). \tag{3}$$

Aside from computation of the porosity and correlation function, the $I(Q)$ data may be analyzed as follows. Scattering from a surface fractal obeys the scaling law $I(Q) \propto Q^{D-6}$, where D is the surface fractal dimension. An alternative fractal analysis is based on the assumption that correlations decay exponentially at length scales greater than ξ [14,15]:

$$I(Q) \propto Q^{-1}\Gamma(5-D)\xi^{5-D}\big[1 + (Q\xi)^2\big]^{(D-5)/2} \times \sin\big[(D-1)\arctan(Q\xi)\big]. \tag{4}$$

Furthermore, assuming that the pore space can be represented by an assembly of independent spherical pores with

an arbitrary distribution $f(r)$ of radii r, the scattering intensity may be computed as

$$I(Q) = (\Delta\rho)^2\phi\frac{\int_{r_{\min}}^{r_{\max}} V_r^2 f(r)F(Qr)\,dr}{\int_{r_{\min}}^{r_{\max}} V_r f(r)\,dr}, \tag{5}$$

where $V_r = (4/3)\pi r^3$ and $F(Qr) = [3\{\sin(Qr) - Qr \times \cos(Qr)\}/(Qr)^3]^2$ are the volume and form factor of spherical scattering objects, respectively. Such a representation, hereafter referred to as the polydisperse spherical pore (PDSP) model, is remarkably useful. This is in part because, as first shown by Schmidt [28] in a prefractal insight, the scattering intensity from the polydisperse system of randomly oriented independently scattering particles follows a power law, which is also ubiquitous for fractal systems. The PDSP model has been numerically tested by Radlinski et al. [29]. For a surface fractal the function $f(r)$ obeys the scaling law $f(r) \propto r^{-(D+1)}$, but the PDSP model is not restricted to fractal microstructures and can be considered as a general representation of the microarchitecture of the rock–pore interface. As will be shown in the next section, several microstructural properties can be directly calculated from this model.

2.2. Experimental techniques

We studied a sandstone sample from an oil reservoir in central Australia. The sample has porosity $\phi = 0.181$ and permeability $k = 450$ mD, as determined by standard core-analysis methods. Mineralogical analysis by X-ray diffraction indicated that the sample contains $98 \pm 0.39\%$ quartz, $0.6 \pm 0.12\%$ dickite, $1.50 \pm 0.37\%$ mica (possibly muscovite), and $0.0 \pm 0.03\%$ montmorillonite. SANS and USANS measurements were performed on a 2-mm-thick sample, using instrument NG7 of the NIST [30] at a wavelength of 5 Å ($10^{-3} < Q < 10^{-1}$ Å^{-1}) and instrument S18 (Austrian beam line, Grenoble Research Reactor, Grenoble, France) [31] at a wavelength of 1.89 Å ($10^{-5} < Q < 10^{-3}$ Å^{-1}), respectively. BSEM images were obtained from polished sections, previously impregnated under vacuum and pressure with a long-chain carbon polymer. The presence of polymer prevents the pores from collapsing in response to mechanical treatment of the rock surface. Sections perpendicular and parallel to the bedding plane were studied (65 images each) using previously reported methods [23], and isotropy of statistical properties was verified. Proton NMR relaxation measurements at 100% water saturation were made on a modified Bruker SXP spectrometer at 26.6 MHz using the Carr–Purcell–Meiboom–Gill pulse sequence [32]. The measured magnetization decay was analyzed according to a multiexponential relaxation model using an inversion algorithm detailed elsewhere [3]. A Micromeritics Poresizer 9310 (60,000 psia maximum pressure) was used to perform the mercury injection porosimetry test on an 1-cm^3 cubic sample, lightly coated with epoxy on all but one face to minimize surface penetration effects.

3. Results and discussion

Typical micrographs of the sample studied are shown in Fig. 1. Fig. 1a displays one of the BSEM images used to determine the correlation function $R_z(r)$. The presence of porosity at multiple length scales is clearly evident in the SEM images shown in Figs. 1b–1d. These images suggest

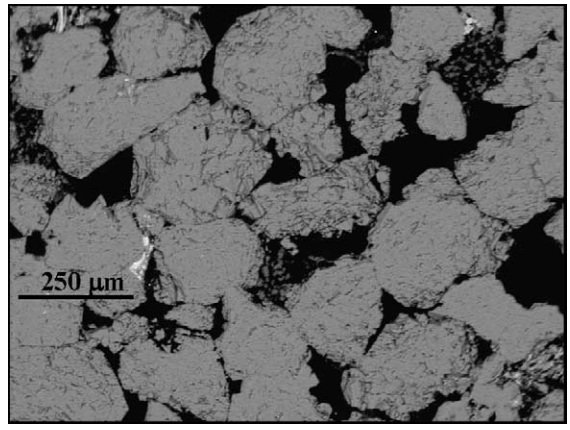

(a)

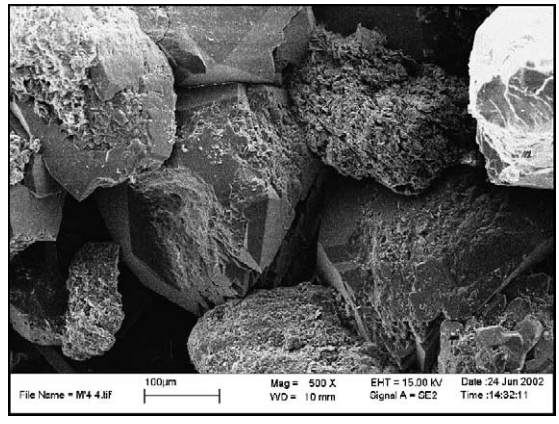

(b)

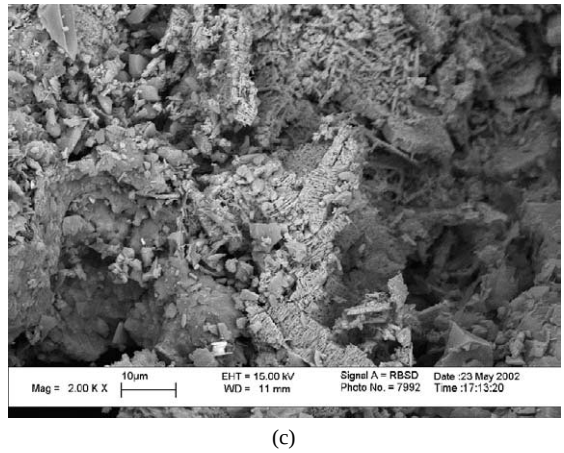

(c)

Fig. 1. (a) Typical BSEM image of impregnated and polished section used for determining the function $R_z(r)$ (magnification 100×: 1.55 µm/pixel). Pore space is shown in black. (b)–(d) SEM images of the sample at increasing magnifications, illustrating the presence of porosity at multiple length scales.

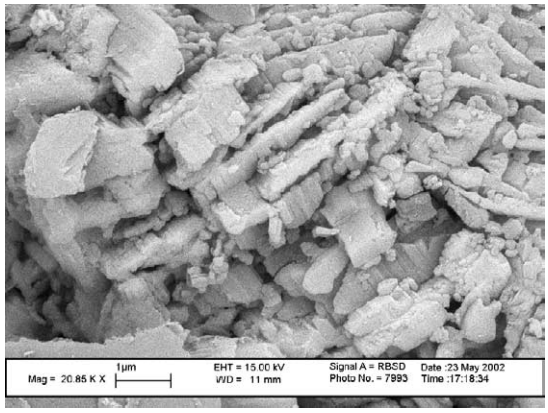

(d)

Fig. 1. (Continued.)

the presence of a hierarchy of pore networks, reminiscent of the multiscale percolation systems envisioned by Neimark [33] and Xu et al. [34].

The combined SANS/USANS/BSEM $I(Q)$ data, depicted in Fig. 2a, span the linear size range from 20 Å to 500 µm, which extends over the entire range of pore sizes in typical sandstones and is the widest continuous range ever studied for a sedimentary rock. These data obey $I(Q) \propto Q^{D-6}$, indicating a very extensive surface fractal system ($D = 2.5$) with an upper cut-off $\xi \approx 50$ µm. At large Q-values ($Q > 0.1$ Å^{-1}), the scattering intensity departs from the ideal power law. This may be due partly to the small-scale compositional inhomogeneities within the rock and partly to the statistical noise related to the relatively low count rate, as the scattering intensity is rapidly decreasing toward the value of the small flat background of 0.006 cm^{-1} (subtracted in Fig. 2a). An analysis of the $I(Q)$ data using Eq. (4), hereafter referred to as the Mildner and Hall (MH) model, yields similar results for the fractal component of the pore space (see Fig. 2a), $D = 2.47$ and $\xi = 35$ µm, but does not accurately describe $R_z(r)$ at large r values (see inset of Figs. 2a and 2b).

Using $(\Delta\rho)^2 = 3.9 \times 10^{10}$ cm^{-2}, we obtain $\phi = 0.184$ from the invariant Y, Eq. (3), and $\phi = 0.181$ from the fit of the PDSP model to the combined $I(Q)$ data—both in excellent agreement with the value ($\phi = 0.181$) determined by a saturation method. The porosity estimated by MP at the maximum intrusion pressure of 60,000 psia ($\phi_{MP} = 0.176$) is also in good agreement. The value $(\Delta\rho)^2 = 3.9 \times 10^{10}$ cm^{-2} used to estimate the porosity from the combined $I(Q)$ data is supported by an independent calculation. Our sample has an apparent grain density of 2.649 g/cm^3, as measured by MP. From X-ray diffraction, the sample composition is approximately 98% SiO_2 (quartz) and 2% $H_2KAl_3(SiO_4)_3$ (muscovite). For this composition and grain density we calculate $(\Delta\rho)^2 = 4.1 \times 10^{10}$ cm^{-2}. The difference between this value and the value used in our computations ($(\Delta\rho)^2 = 3.9 \times 10^{10}$ cm^{-2}) is 5%. This difference is within the error of SANS/USANS data, which is estimated to be ±5%.

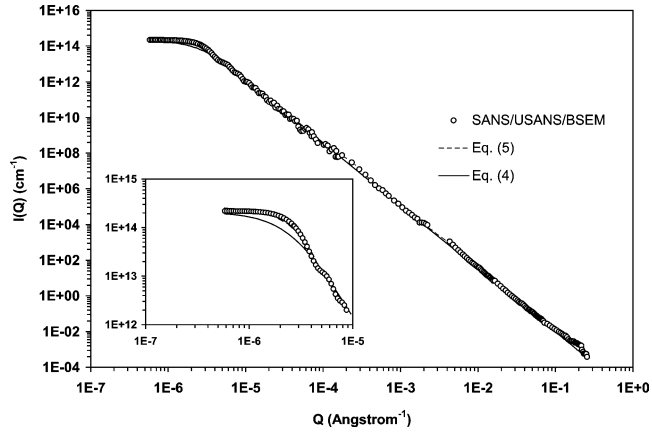

(a)

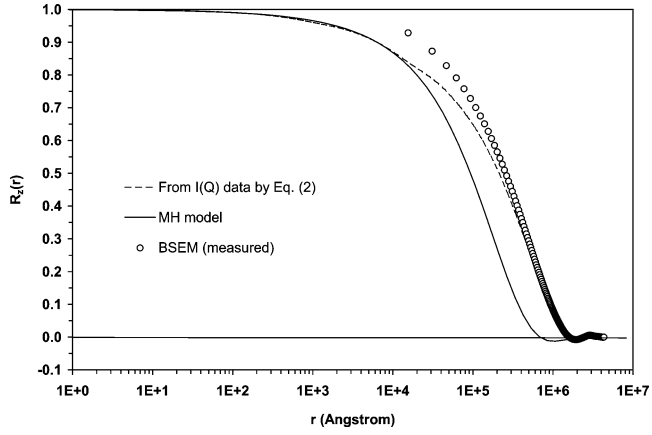

(b)

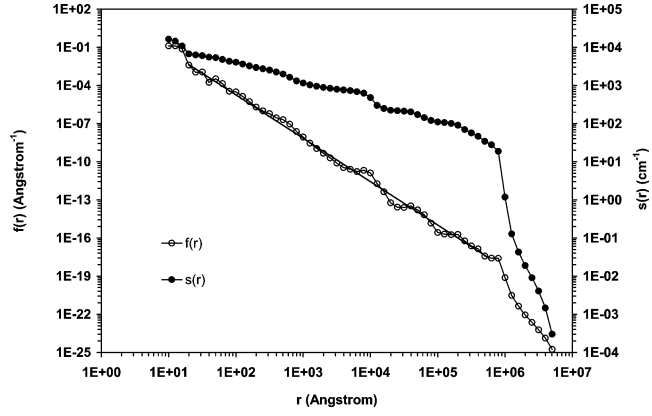

(c)

Fig. 2. (a) Absolute neutron-scattering cross section $I(Q)$ (after background subtraction of 6×10^{-3} cm^{-1}) and (b) correlation function $R_z(r)$ from combined SANS/USANS/BSEM data and models (see text for details). Contributions to $R_z(r)$ by nonfractal objects of size $r > 50$ µm are apparent. (c) Distributions of pore size, $f(r)$, and specific surface area, $s(r)$. Straight line corresponds to $f(r) \propto r^{-(D+1)}$ with $D = 2.49 \pm 0.03$.

As shown in Fig. 2c, the pore-size distribution according to the PDSP model, Eq. (5), follows $f(r) \propto r^{-(D+1)}$ with $D = 2.49 \pm 0.03$ for 20 Å $\leqslant r \leqslant$ 55 µm, in agreement with the other estimates. Remarkably, the fraction of the pore volume associated with the surface fractal regime

is approximately 62%. The specific surface area, s, at a pore size of 10 Å is 1.64 μm^{-1} according to the PDSP model (see Fig. 2c)—of the same order of magnitude as the value determined by MP ($s = 0.47\ \mu m^{-1}$), but higher since MP does not account for contributions to the surface area by pores smaller than about 20 nm.

For locally spherical solid–void interface geometry, as assumed in writing Eq. (5), the relationship between capillary pressure and pore size is the well-known Young–Laplace equation, $P_c = 2\sigma\cos\theta/r_t$, where σ is the surface tension, θ is the receding contact angle, and r_t is the radius of pore *throats* (volumeless local constrictions in the pore space) through which pore *bodies* are accessible to a nonwetting liquid [1]. Since $f(r)$ must be identified with the pore *body* size distribution, the experimental mercury intrusion data are quantitatively consistent with an average pore body-to-throat size ratio $\langle r/r_t\rangle \approx 3.5$ (see Fig. 3a). This value agrees remarkably well with recent independent estimates of the pore-to-throat aspect ratio for sandstone rocks of similar lithology, porosity, and permeability [35]. Further support for the validity of pore structure information extracted by the application of the PDSP model to the combined SANS/USANS/BSEM data is provided below.

As shown in Fig. 3b, measurement of the decay of nuclear transverse magnetization in the water-saturated sample shows a distinctively bimodal distribution of T_2 relaxation times. This behavior is consistent with a model of NMR relaxation in fractal pores [36]. According to this model, at distance L_{cg} from the pore walls, a Minkowski frontier delimits inner pore volumes of size L_{int}. Nuclear spins within a distance L_{cg} from the pore walls (the so-called "coarse-graining" length) diffuse easily to the surface and are relaxed with characteristic time $T_{2,short} \approx L_{cg}^2/D_0$, where $L_{cg} = \ell(\Lambda/\ell)^{1/(D-1)}$, $\Lambda = D_0/\rho$, ℓ is the lower cutoff of the fractal region, D_0 is the self-diffusion coefficient of water, and ρ is the surface relaxivity. The fraction of magnetization that follows this rapid decay is $f_{short} = (L_{cg}/\xi)^{2-D}$, where ξ is the upper cutoff of the fractal region. Relaxation of spins within the inner pore volume is diffusion-controlled and has characteristic time $T_{2,long} \approx L_{int}^2/(2\pi^2 D_0)$. Using $D = 2.47$ and $\ell = 2$ nm from our SANS measurements, $D_0 = 2.5\times10^{-9}$ m^2/s, $\rho = 12$ μm/s [37,38], and for the experimentally observed relaxation times ($T_{2,short} \approx 0.01$ s, $T_{2,long} \approx 0.1$ s) and peak intensities ($f_{short} = 0.41$, $f_{long} = 0.59$), we predict $\xi \approx 35$ μm and $L_{int} \approx 75$ μm. These estimates are consistent with our analysis of scattering data. Since for the above parameter values $L_{cg} = 5$ μm, we may further attempt to *predict* f_{short} from the pore size distribution $f(r)$ of Fig. 2c, as follows:

$$f_{short} = \frac{\int_{r_{min}}^{L_{cg}} r^3 f(r)\,dr + \int_{L_{cg}}^{r_{max}} [r^3 - (r - L_{cg})^3] f(r)\,dr}{\int_{r_{min}}^{r_{max}} r^3 f(r)\,dr}. \tag{6}$$

This calculation gives $f_{short} = 0.47$, in good agreement with the NMR experiment.

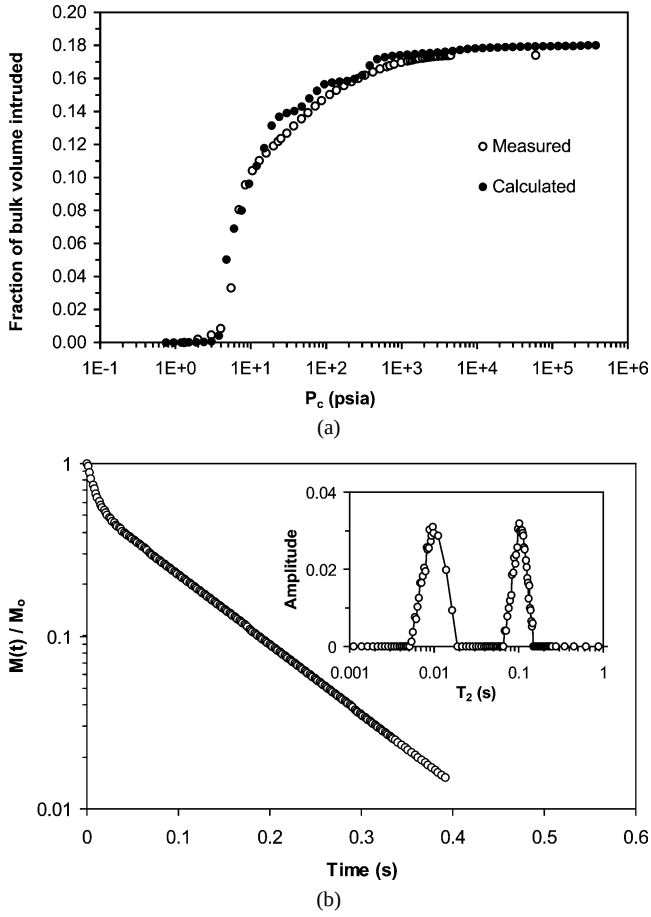

Fig. 3. (a) Measured and calculated mercury intrusion porosimetry curve. Pore volumes calculated as $V_r = (4/3)\pi r^3$ from pore *body* sizes r distributed according to $f(r)$ (see Fig. 2c). Capillary pressures calculated from the Young–Laplace equation for surface tension $\sigma = 485$ mN/m, receding contact angle $\theta = 40°$, and pore *throat* size $r_t = r/3.5$. (b) Decay of transverse nuclear magnetization $M(t)/M_0$ in water-saturated sample. The distribution of T_2 relaxation times (inset) is consistent with a model of surface-enhanced relaxation in fractal pores [36].

We finally note that the length scale l_c (pore throat diameter) controlling flow permeability k may be estimated from the relationship $k = l_c^2/(226F)$ [39], where F is the electrical formation factor. For our sample, $k = 450$ mD, $\phi = 0.181$, and using $F = \phi^{-m}$ (Archie's law) with $1.8 \leqslant m \leqslant 2$, we obtain $l_c = 52 \pm 4$ μm, corresponding to a pore throat radius of 26 ± 2 μm. The mercury–air breakthrough capillary pressure computed from the Young–Laplace equation for this radius, $P_c^0 = 4.2 \pm 0.3$ psia, is in very good agreement with the experimental porosimetry data (see Fig. 3a). For a pore-body-to-throat aspect ratio of 3.5, the associated pore-body radius is 91 ± 7 μm, which corresponds well with L_{int} determined by analysis of the NMR relaxation data.

4. Conclusions

In this paper, we proposed and tested the statistical fusion of experimental small-angle neutron scattering (SANS

and USANS) and backscatter SEM imaging data of porous media and their subsequent interpretation in terms of a polydisperse spherical pore (PDSP) model. Our objective was to probe quantitatively the entire spectrum of pore-length scales within a sample of reservoir sandstone. We found that the sample studied is an extensive (ca. 62% of the pore volume) surface fractal ($D = 2.47$) in the pore-size range 10 Å–50 μm and is Euclidean for larger length scales. The pore-size distribution according to a fit of the PDSP model to the combined SANS/USANS/BSEM data agreed quantitatively with the measured NMR response of the water-saturated sample, within the context of a model of spin relaxation in fractal pores [36]. The derived pore-size distribution also reproduced the mercury intrusion porosimetry curve, assuming an average pore-to-throat size aspect ratio of about 3.5. This a value agreed with estimates obtained independently by Song [35] for samples of similar lithology, porosity, and permeability. From these results we conclude that the proposed multiscale statistical-geometric description furnishes useful and unifying insights into the pore-size distribution, porosity, and correlation function and the characteristic length scales for capillary pressure, nuclear spin relaxation, and flow permeability. The proposed method may find use in the characterization of other materials exhibiting broad pore-size distributions, such as carbonate rocks, soil, cements, and concretes and should be a useful complement to alternative techniques, which rely on solid–fluid interactions for pore structure characterization [40,41]. The method may also provide detailed input data (two-point correlation functions) for the computer reconstruction [42,43] of the microstructure of porous rock and other materials exhibiting both fractal and Euclidean characteristics.

Acknowledgments

The financial support provided by the Natural Sciences and Engineering Research Council of Canada (NSERC) to M.A. Ioannidis for this research is gratefully acknowledged. A.P. Radlinski and A.L. Hinde publish with the permission of the CEO, Geoscience Australia.

References

[1] F.A.L. Dullien, Porous Media: Fluid Transport and Pore Structure, second ed., Academic Press, San Diego, 1992.
[2] M. Sahimi, Rev. Mod. Phys. 65 (1993) 1393.
[3] D. Chang, M.A. Ioannidis, J. Colloid Interface Sci. 253 (2002) 159.
[4] C.D. Tsakiroglou, A.C. Payatakes, J. Colloid Interface Sci. 159 (1993) 287.
[5] S. Bekri, J. Howard, J. Muller, P.M. Adler, Transp. Porous Media 51 (2003) 41.
[6] G.N. Constantinides, A.C. Payatakes, Transp. Porous Media 38 (2000) 291.
[7] B. Mandelbrot, The Fractal Geometry of Nature, second ed., Freeman, New York, 1983.
[8] P. Pfeifer, D. Avnir, J. Chem. Phys. 79 (1983) 3558.
[9] A.J. Katz, A.H. Thompson, Phys. Rev. Lett. 54 (1985) 1325.
[10] C.E. Krohn, J. Geophys. Res. 93 (1988) 3297.
[11] A.H. Thompson, Ann. Rev. Earth Planet. Sci. 19 (1991) 237.
[12] C.G. Jacquin, P.M. Adler, Transp. Porous Media 2 (1987) 571.
[13] J.P. Hansen, A.P. Skjeltorp, Phys. Rev. B 38 (1988) 2635.
[14] H.D. Bale, P.W. Schmidt, Phys. Rev. Lett. 53 (1984) 596.
[15] D.F.R. Mildner, P.L. Hall, J. Phys. D Appl. Phys. 19 (1986) 1535.
[16] P.-Z. Wong, A.J. Bray, Phys. Rev. Lett. 60 (1988) 1344.
[17] P.-Z. Wong, J. Howard, J.-S. Lin, Phys. Rev. Lett. 57 (1986) 637.
[18] M.H. Cohen, in: Physics and Chemistry of Porous Media II, in: AIP Conference Proceedings, vol. 154, 1987.
[19] D. Avnir (Ed.), The Fractal Approach to Heterogeneous Chemistry: Surfaces, Colloids, Polymers, Wiley, Chichester, 1989.
[20] A.P. Terzyk, P.A. Gauden, P. Kowalczyk, Arabian J. Sci. Eng. 28 (1C) (2003) 133.
[21] S. Bakke, P.E. Oren, SPE J. 2 (1997) 136.
[22] S.C. Blair, P.A. Berge, J.G. Berryman, J. Geophys. Res. B 101 (9) (1996) 20359.
[23] M.A. Ioannidis, M.J. Kwiecien, I. Chatzis, J. Pet. Sci. Eng. 16 (1996) 251.
[24] P. Spanne, J. Thovert, C. Jacquin, W. Lindquist, K. Jones, P.M. Adler, Phys. Rev. Lett. 73 (1994) 2001.
[25] T. Fredrich, B. Menendez, T.-F. Wong, Science 268 (1995) 276.
[26] A.P. Radlinski, E.Z. Radlinska, M. Agamalian, G.D. Wignall, P. Lindner, O.G. Randl, Phys. Rev. Lett. 82 (1999) 3078.
[27] P.M. Adler, C.G. Jacquin, J.A. Quiblier, Int. J. Multiphase Flow 16 (1990) 691.
[28] P.W. Schmidt, J. Appl. Crystallogr. 15 (1982) 567.
[29] A.P. Radlinski, C.J. Boreham, P. Lindner, O. Randl, G.D. Wignall, A.L. Hinde, J.M. Hope, Org. Geochem. 31 (2000) 1.
[30] C.J. Glinka, J.M. Rowe, J.G. LaRock, J. Appl. Crystallogr. 19 (1986) 427.
[31] M. Hainbuchner, M. Villa, G. Kroupa, G. Bruckner, M. Baron, H. Amenitsch, E. Seidl, H. Rauch, J. Appl. Crystallogr. 33 (2000) 851.
[32] R.L. Kleinberg, in: D.M. Grant, R.K. Harris (Eds.), Encyclopedia of Nuclear Magnetic Resonance, Wiley, New York, 1996.
[33] A.V. Neimark, Sov. Phys. JETP 69 (1989) 786.
[34] K. Xu, J.-F. Daian, D. Quenard, Transp. Porous Media 26 (1997) 51.
[35] Y.-Q. Song, Magn. Reson. Imaging 19 (2001) 417.
[36] B. Sapoval, S. Russ, D. Petit, J.P. Korb, Magn. Reson. Imaging 14 (1996) 863.
[37] W.F.J. Slijkerman, J.P. Hofman, Magn. Reson. Imaging 16 (1998) 541.
[38] K.J. Dunn, D.J. Bergman, G.A. LaTorraca, in: K. Helbig, S. Treitel (Eds.), Nuclear Magnetic Resonance Petrophysical and Logging Applications, in: Handbook of Geophysical Exploration, vol. 32, Pergamon, Amsterdam, 2002.
[39] A.H. Thompson, A.J. Katz, C.E. Krohn, Adv. Phys. 36 (1987) 625.
[40] Y.-Q. Song, S.G. Ryu, P.N. Sen, Nature 406 (2000) 178.
[41] D. Broseta, L. Barre, O. Vizika, N. Shahidzadeh, J.-P. Guilbaud, S. Lyonnard, Phys. Rev. Lett. 86 (2001) 5313.
[42] Z. Liang, M.A. Ioannidis, I. Chatzis, Chem. Eng. Sci. 55 (2000) 5247.
[43] J.-F. Thovert, F. Yousefian, P. Spanne, C.G. Jacquin, P.M. Adler, Phys. Rev. E 63 (2001) 061307.